

Electronic Theses and Dissertations, 2004-2019

2018

Mechanism Design of a Compact 4-DOF Robotic Needle Guide for MRI-Guided Prostate Intervention

Shihao Zhang
University of Central Florida

 Part of the [Electro-Mechanical Systems Commons](#)
Find similar works at: <https://stars.library.ucf.edu/etd>
University of Central Florida Libraries <http://library.ucf.edu>

This Masters Thesis (Open Access) is brought to you for free and open access by STARS. It has been accepted for inclusion in Electronic Theses and Dissertations, 2004-2019 by an authorized administrator of STARS. For more information, please contact STARS@ucf.edu.

STARS Citation

Zhang, Shihao, "Mechanism Design of a Compact 4-DOF Robotic Needle Guide for MRI-Guided Prostate Intervention" (2018). *Electronic Theses and Dissertations, 2004-2019*. 5825.
<https://stars.library.ucf.edu/etd/5825>

DESIGN AND MOTION CONTROL OF A FOUR DEGREE OF FREEDOM ROBOTIC
NEEDLE GUIDE FOR MRI-GUIDED INTERVENTION

by

SHIHAO ZHANG
B.S. Central Michigan University, 2015

A thesis submitted in partial fulfillment of the requirements
for the degree of Master of Science
in the Department of Mechanical and Aerospace Engineering
in the College of Engineering & Computer Science
at the University of Central Florida
Orlando, Florida

Spring Term
2018

Major Professor: Sang-Eun Song

ABSTRACT

In the past several MRI compatible robotic needle guide devices for targeted prostate biopsy have been developed. The large and complex structure have been identified as the major limitations of those devices. Such limitations, in addition to complex steps for device to image registration have prevented widespread implementation of MRI-guided prostate biopsy despite the advantages of MRI compared to TRUS.

We have designed a compact MRI-guided robotic intervention with the capability to have angulated insertion to avoid damage to any anatomical feature along the needle path. The system consists of a novel mechanism driven Robotic Needle Guide (RNG). The RNG is a 4-DOF robotic needle manipulator mounted on a Gross Positioning Module (GPM), which is locked on the MRI table. The RNG consists of four parallel stacked disks with an engraved profile path. The rotary motion and positioning of the discs at an angle aids in guiding the biopsy needle. Once a clinician selects a target for needle insertion, the intervention provides possible insertion angles. Then, the most suitable angle is selected by the clinician based on the safest trajectory. The selected target and insertion angle are then computed as control parameters of RNG i.e. the discs are then rotated to the required angle. Insertion is followed by quick confirmation scans to ascertain needle position at all times.

ACKNOWLEDGMENTS

I would like to appreciate Dr. Sang-Eun Song for the research opportunity, for involvement in the important project in the intervention robotics lab and for his support during my research.

To my committee members, Dr. Yunjun Xu and Dr. Ulas Bagci, for their time and valuable feedback.

To my friends, Mr. Pradipta Biswas for his research support and interest in further development of this project, Mr. Pankaj Kulkarni and Mrs. Sakura Sikander for their support and comments on this project. Miss. Leslie Simms for documenting the research.

TABLE OF CONTENTS

CHAPTER 1 INTRODUCTION	1
1.1 Background.....	1
1.2 MRI Compatible Motor	4
CHAPTER 2 DESIGN CONCEPT	9
2.1 Principle Mechanism	9
2.1.1 Realization of design concept – motion transfer	9
2.1.2 Curve profile.....	13
2.1.3 Origin of Curve Developments.....	16
2.1.4 Issue with Center of Disks	19
2.2 Design development	20
CHAPTER 3 CONTROL SYSTEM.....	21
3.1 Motion Control	21
3.1.1 Decoupled simple motion control.....	21
3.1.2 Continuous motion control	22
3.2 Homing Control	25
CHAPTER 4 DISCUSSION.....	27
CHAPTER 5 CONCLUSION.....	30
APPENDIX A PREVIOUS DESIGNED MECHANISM.....	31
A APPENDIX B SOLID WORK MOTION STUDY.....	33

LIST OF FIGURES

Figure 1-1 Prostate Cancer Detecting Images (a) typical TRUS, and (b) various multi parametric MRI for lesion identification.	2
Figure 1-2 Schematic of the Prostate Biopsy under MRI environment[15]	4
Figure 2-1 Illustration of the Mechanism Principle	10
Figure 2-2 Connection between Ball Joint and Groove – The First Motion transfer	11
Figure 2-3 Schematic of Disk and Grooves	13
Figure 2-4 Illustration of few Design Discussion, (a) is linear shape (b) and (c) are linear shape with bending interruption, (d) is a half circle, (e) and (f) is for the center point discussion	17
Figure 3-1 Two Simple Motion (a) Parallel Rotation, (b) Parallel Radius Motion	21
Figure 3-2 Configuration of Motion Study Setup	24
Figure 3-3 Homing System Setup	26
Figure 5-1 Previous Design Mechanism	32
Figure 5-2 Disk 1 Dynamic for a Horizontal Linear Path	34
Figure 5-3 Disk 2 Dynamic for a Horizontal Linear Path	34
Figure 5-4 Disk 3 Dynamic for a Horizontal Linear Path	34
Figure 5-5 Disk 4 Dynamic for a Horizontal Linear Path	34
Figure 5-6 Circuit connection for E32 Optical Sensor	34
Figure 5-7 Oscilloscope Reading from the E-3-X Amplifier (a) Higher Reflection Detected, (b) Lower Reflection Detected	34

CHAPTER 1 INTRODUCTION

1.1 Background

Prostate cancer is the third leading cause of cancer related deaths in The United States, and sixth worldwide [3]. To avoid spreading of cancer, early diagnosis is critical for timely treatment. Different methods exist for diagnosis and treatment of the prostate cancer. One of the surgical treatment options is radical prostatectomy. During this surgical operation, the entire prostate gland plus some of the tissue around it is removed. Radiation therapy is another method for the treatment that uses high-energy rays or particles to kill cancer. Nevertheless, all these treatment methods rely on proper diagnosis. The early diagnosis is even more critical considering the patient survival and avoiding detrimental late-stage treatments such as chemotherapy, which is a method to inject drugs into the entire bloodstream [4]. According to U.S. Preventive Services Task Force, the early detection of cancer would dramatically decrease the chance of deaths from prostate cancer by 40 percent [5].

However, as a critically significant procedure in the prostate cancer, the current diagnosis method has certain limitations. The current standard and most common diagnosis method for prostate cancer is Transrectal Ultrasonography (TRUS)-Guided Biopsy [6]. In this method ultrasonography is used to determine the cancer existence and tumor location. By using the US image, the patient's prostate and anatomical features around it are identified. Then, the clinician inserts a biopsy needle to the prostate around 6 to 12 locations roughly covering entire prostate to sample tissues [7] for diagnosis. In transperineal approach, the needle is often inserted through a guidance template which consists of grid of holes, which allows the needle to be guided and inserted into the prostate [6]. Computed tomography (CT) is another imaging method for prostate cancer detection [8]. As

for the prostate cancer, the CT scan will focus on the pelvic region to localize the lesion, including prostate, bladder, rectum, anal canal, and seminal vesicles. Another method is to use MRI (Magnetic resonance imaging) for prostate cancer diagnosis.

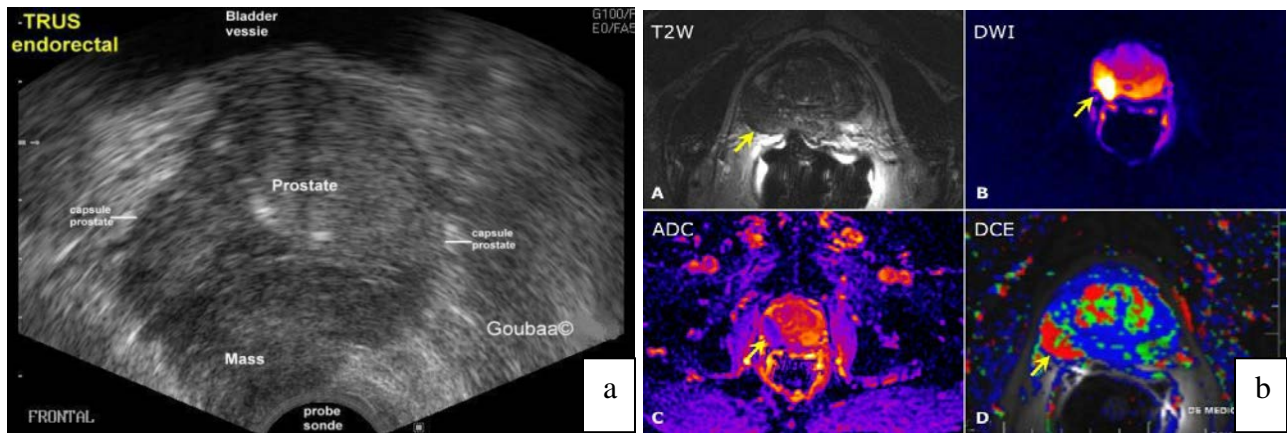


Figure 1-1 Prostate Cancer Detecting Images (a) typical TRUS, and (b) various multi parametric MRI for lesion identification.[1, 2]

The MRI detection is more reliable compared to US or CT detection. According to recent research, MRI is more accurate than TRUS-biopsy in terms of both sensitivity and negative predictive value. The false-negative rate of current TRUS-guided system is commonly 21~47%. MRI imaging system has a potential to reduce the false-negative percentage [9]. Compared with TRUS, MRI image can show cancer suspicious tissue much clearly, thus, the detection accuracy guided by the MRI imaging system is much better than the TRUS procedure. Research shows that when detecting significant prostate cancer, the sensitivity of MRI guidance biopsy detection is 20% more than the current standard US detections [10]. Typically, the cancer detection rates of TRUS-guided biopsy is about 22% to 29%, the MRI targeted biopsy has a detection rates of 38% to 59% [11]. For MRI prostate intervention, a few needle guidance systems have been introduced [12-14]. For

example, Hata et al at Brigham and Women's Hospital and Harvard Medical School developed an MRI compatible manual needle guided. It has 3-DOF for positioning the needle [13].

Robotic needle guidance has also been studied, such as the MrBot [15]. It is a robotic needle guide, which is actuated by pneumatic motors. It permits 5-DOF needle motion. Recently MrBot received FDA clearance for clinical applications. Another robotic needle guide system is the Smart Template [16]. The Smart Template can deliver 2-DOF motion by using ultrasound motors. Both of these robotic systems could be used safely under the MRI environment.

Although the MRI treatment is a better approach for prostate cancer detection, MRI guided biopsy systems developed in past are either bulky or don't allow angulated needle insertion. Along with addressing these issues, the accuracy requirement of such devices is also critical for diagnosis. In conclusion, a high level of precision, compact mechanism and angulated insertion have been identified as crucial requirements in MRI guided targeted biopsies.

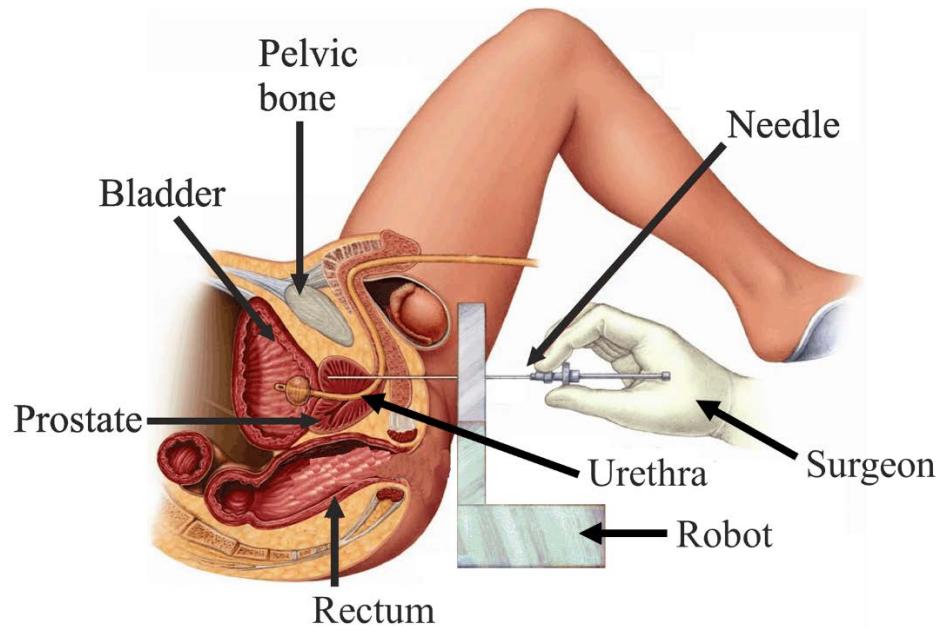


Figure 1-2 Schematic of the Prostate Biopsy under MRI environment[17]

Hence, considering above challenges in existing systems, a novel MRI guided 4-DOF needle guide mechanism has been designed. The mechanism consists of two sets of double disks, which enable needle positioning. The 4-DOF permits maximum 15 degrees of needle angulation in the current design.

1.2 MRI Compatible Motor

The system presented in this study is designed to operate under the MRI environment. MRI system is characterized by powerful magnetic field, radio waves and a computer console to produce detailed images of the inside of human body [18]. It is used to in diagnosis or monitoring of a variety of diseases in chest, abdomen and pelvis, including breast and ovarian cancer [19]. As discussed earlier, for the application of prostate cancer diagnosis MRI has been proved to be a better method than TRUS. Several researchers in past have proved the feasibility of MRI-guided

prostate cancer detection using MR compatible intervention systems. One of the limitations of those systems is the bulky design and large footprint in the MR room [20], which is not favored by operating clinicians since the space in the MRI bore is limited. A major concern for the robotic system, operating under MRI environments, is the interruption in the magnetic field due to its presence. Most of the commercialized motors and encoding systems produce its own magnetic field. These actuators cannot be used in the MRI environment, since it would interrupt the magnetic field of the MRI system and distort the image. Hence, for our interest, a different actuation technology is needed to minimize any of the magnetic components.

To develop a robotic system, which is able to operate properly under the MRI environment, it is fundamental to utilize special actuators that are able to run under MRI environment. Currently, there are two types of motors can be used for such requirements. These are the pneumatic actuator and piezoelectric actuator [21, 22]. A pneumatic motor, which is clean and safe under the MRI environment, consists of a complex mechanism structure (such as a gearbox) to convert the air pressure to accurate motion. For example, The MrBot mention above[15]r et al However, the robot accuracy using this type of motor is heavily relying on high ratio gearbox, which conflicts with our approach to design a simplified system.

The piezoelectric motor deforms driving elements by applying an internal electric field [23]. By manipulating the piezo-effect generated from typical ceramic (piezo ceramic), the driving elements in a piezoelectric motor could move either as a linear actuator or rotary actuator. Piezo motors do not require a magnetic field to operate, which makes it a good candidate for the MRI environment. Compared to pneumatic motors, piezo motor has several advantages [16]. Compared to pneumatic motors in which the motions are controlled by air pressure, the piezo motor is much more reliable

for higher accuracy. The resolution of a commercial piezo motor is around 100nm[24]. On the other hand, a typical resolution for a linear pneumatic motor is from 12 mm to 25 mm [25] compared to a piezo motor which has almost thousands times better resolution [26]. The pneumatic motor is also not able to compete with the piezo motor under consideration of accuracy.

For the clinical setting, the non-back-drivable system is extremely important. A non-back-drivable system is not able to move by external force after they have been moved to a desired position, even when power has been cut off. This characteristic can be significantly valuable for clinician. The piezo effect mentioned above is directly related with the material property, which means, after a certain position have been attained by a piezo motor, even in the case when electrical power goes down, the piezo motor will not slide back or change its position [24]. This characteristic fulfill the desired feature in clinical setting and has also been emphasized when designing the mechanical system. The high energy density contained within piezo motors results in its smaller consumption of energy when compared to DC motors. Additionally, piezo motors do not require application of high-ratio gearbox to achieve a high accuracy, resulting in lower mechanical losses. A typical piezo motor consumes 40% less energy compared to a traditional motor in the same working condition [27].

Piezoelectric motors have been already commercially developed and is a well-established technology. Currently there are some other motors that also operate under the principle of piezoelectric effect, thus, could be used under the MRI environment. They are ultrasound motors and piezo inertial motors.

Piezoelectric inertia drivers have a high holding force compared with other types of piezoelectric motors. This is mainly due to the stick-slip effect (inertia effect). This type of motor also has a

non-back-drivable design, which means that after power is cut down, the piezo inertia driver will self-lock its position at that point without slip back. A drawback of this type of motor is that the speed of movement is only 5mm/s. Ultrasonic piezo motors work somewhat similar to Piezo LEGS motors [ref]. The piezoelectric actuator deforms periodically to deliver driving forces to the running component, however, the difference is that the actuator is running in ultrasonic vibrations with a high-frequency AC voltage between 100 to 200 kHz. This high feeding frequency generates relatively high velocities, which can reach 500mm/s. The main drawback for this kind of motor is that the holding torque is only 0.3Nm. Piezo motor can have two variations: piezo linear motor and piezo rotary motor. Most of the piezo linear motors have a limited travel length, however by different designs and rotary configuration, the travel length of a Piezo LEGS motor could reach infinite. Examples include Nano motion HR series motors and LS series motors [ref]. As for other motors, most of the ultrasonic piezo motor and inertia drives are the rotary motor [24, 28].

As mentioned above, piezo motors could adapt into many medical applications due to the advantages of MRI compatibility, size and accuracy. There are many previous examples of medical devices which use piezoelectric motors.

Due to the considerations above, we decided to use piezoelectric motor to build a compatible guidance device under the MRI environment. By utilizing the advantages of the piezo motor, it become feasible to develop the concept of high accuracy guidance mechanism with an adaptable size, and at the same time, could be used under the MRI environment.

The piezo motor selected for this application is a type of Piezo LEGS motor. It is commercially available from “Piezo Motor” [28]. Previously, we developed a mechanism by using the piezo motor provided from Nano motion. It is a piezo motor with infinite linear range. However, the

previous design has been dismissed due to the consideration of sliding. At this point, we iterated another design by using the current rotary motor. We decided to use the timing belt to connect the rotary motor and mechanism components. Compared to previous design, instead of relying on the friction force to actuate the mechanism, the timing belt design is more reliable. While considering this design the emphasis was on the characteristic of non-back-drivability. The timing-belt design is also more practical than previous design.

CHAPTER 2 DESIGN CONCEPT

2.1 Principle Mechanism

The design needs to be MRI compatible, small size and also has a reasonable resolution. Considering these, we designed a unique mechanism unlike other traditional guidance systems. The conventional guidance system is mostly based on Cartesian coordinate, however this system utilizes polar coordinate principle to guide the needle position. This means position in our mechanism is transferred into a function of angle and radius. In this system, needle biopsy can have 2-D motion on its axis plane and is able to create angular manipulation related to the axis by individually controlling two control planes.

In current TRUS based diagnosis, biopsy needle is often guided into the prostate through the perineum, avoiding the pubic arch and other anatomical features [29]. The system we developed can provide a more accurate needle placement by benefiting from the robotic system. The capability of angulation of the needle is also an important advantage of the system.

2.1.1 Realization of design concept – motion transfer

The principle of this design is shown in the figure below, the needle guide design consists of two sets of disks, two ball joints and the biopsy needle will insert through the ball joints.

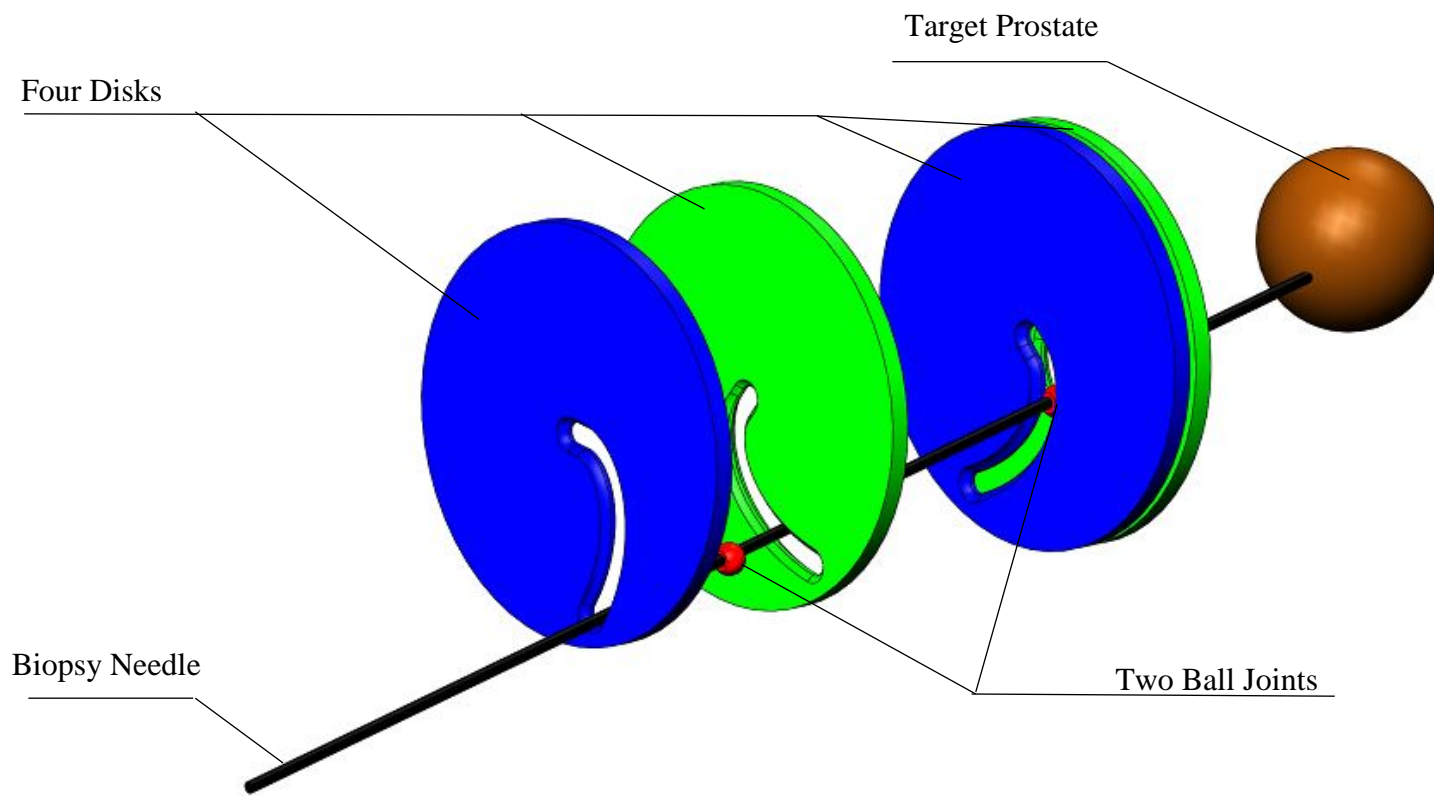


Figure 2-1 Illustration of the Mechanism Principle

The ball joints fit in between the double disk. During the rotation, the ball joints are directed by the intersections of the grooves, the connection of ball joint would make the needle rotate smoother since the outer surface of the ball joint have less friction with the groove and the inner side of the ball joint would stable the needle guide.

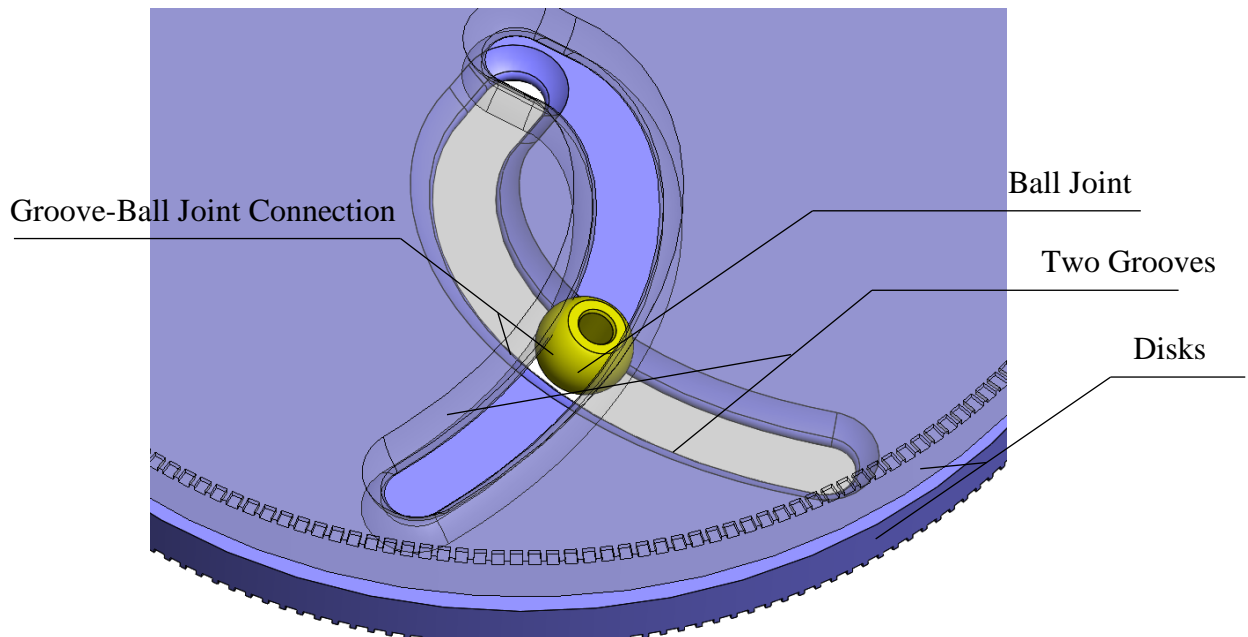


Figure 2-2 Connection between Ball Joint and Groove – The First Motion transfer

To explain the motion principle, it is important to realize each motion transfer throughout the whole design. From the view of motion transfers, starting from needle guide motion back to the motors that drive it. There are three motion transfers for this apparatus: (i) the ball joint oriented by the curvature grooves; (ii) the curvature grooves move with the circular disks; and (iii) the circular disks driven by the motors.

For the first motion transfer, between ball joints and the grooves, this motion transfer moves the ball joints on a pre-calculated path. The orientation of needle is restricted by two points in the space, each of those points is determined by the intersection of two grooves in a fixed frame. By

the effort of two ball joints, the needle position can be controlled by the grooves. By literature reference, 15 degrees angular should be sufficient for the prostate biopsy. Thus, the whole mechanism is designed to accomplish such purpose.

The second motion transfer, each groove has been drawn and cut on one of the circular disks. Thus, the grooves are carried by the rotation of disks. As stated above, the intersection of two grooves will be used to control the ball joint in a fixed frame. Hence, two circular disks featured by the grooves can be used for a 2-DOF needle control. In other words, one set of disk mechanism is able to provide 2-DOF movement. By arranging two sets of double disks parallel to each other, and coincident to each other relative to the common axis of disks, the mechanism should be able to provide a 4-DOF needle guidance. For the disk design, beside with groove profile, the edge of the disk also need to be modified for a timing belt to fit around it, which will be explained in next paragraph.

The last motion transfer is between the disks and motors. We had come up with many ideas to deliver rotations to the disk. Eventually we decided to use the timing belt to connect the motor shaft and edge of disk as introduced in chapter 1. Hence, 4 motors are required for this mechanism. Each motor will provide rotational motion to a specified disk. The frames of double disks and motors will settle on a distance-fixed base, which means, the distance between two sets of double disks is constant. Thus, the needle path for this mechanism is unique in space. The entire mechanism is therefore connected by four independent frames and a base. The base will horizontally laid on a flat surface, the frames will be vertically constructed on the base. Each frame has an independent set of motor and disk, each motor will be driven by an individual control axis

2.1.2 Curve profile.

The essential of guidance system is double disk and the groove profile in the second motion transfer.

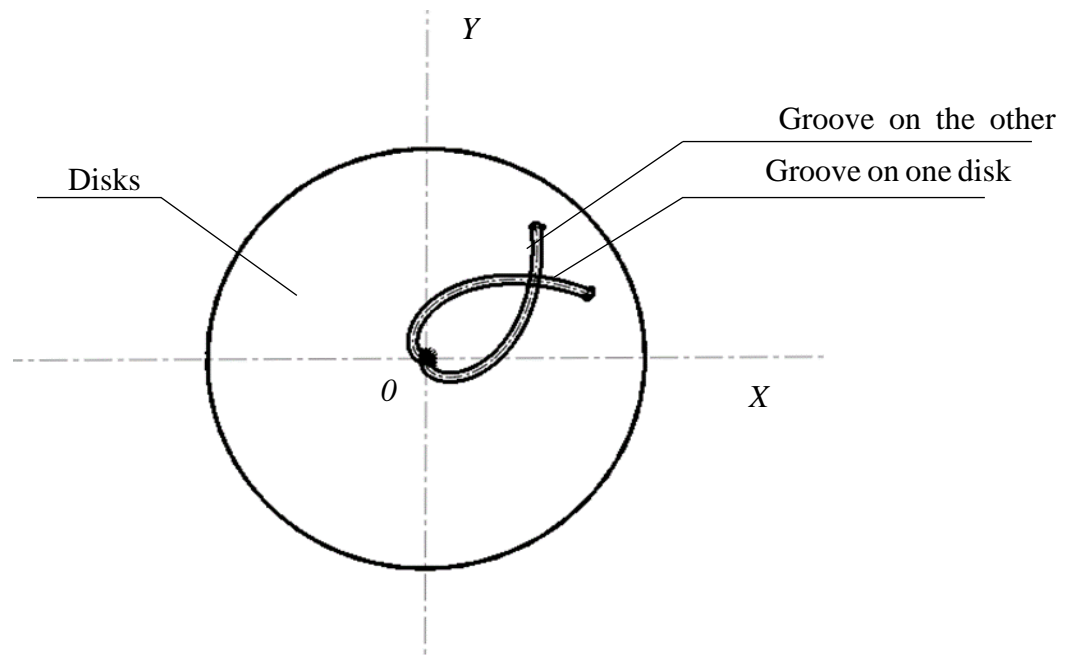


Figure 2-3 Schematic of Disk and Grooves

As shown in figure 2-3, two grooves are relatively perpendicular to each other. Such perpendicularity remains as long as the grooves rotate along its common axis. Thus, theoretically, the intersection of two grooves will also remain in a relatively consistent square shape to hold the ball joint statically. By a different groove profile, the shape of intersection can be variables. Although in this design, the grooves profiles we used can fix the shape of intersection. From the functional perspective, the shape of the intersection does not require to be fixed. As long as it can carry the ball joint tight, the shape of intersection also could be other different shapes. This part will be discussed in the later section.

The specific curved profile of the groove is very important, since this profile needs to be perpendicular with each other when two of them intersects in a set of disc. To understand this curve profile, it is necessary to know the origin of such curve. The concept of orthogonal trajectory, for a curve that intersects every member of a one parameter family of curves orthogonally (at right angles) is called an orthogonal trajectory. The curves we used is one set of orthogonal trajectories. Mathematically, orthogonal trajectories are perpendicular to each other. The condition for general equation to have an orthogonal trajectory is when the differentials of those equation multiplied to be -1. As equations shows below

General equation:

$$F(x, y) = 0 \quad (1)$$

Differential equation

$$\frac{dy}{dx} = f(x, y) \quad (2)$$

Orthogonal differential equation

$$\frac{dy}{dx} = \frac{-1}{f(x, y)} \quad (3)$$

In our case, when the general polar equation for one curve is:

$$x = e^t \cos t \quad (4)$$

$$y = e^t \sin t \quad (5)$$

(The t here is a factor of curve length and curve turning angle, normally within the range of $0 \leq t < 1.57$, this also apply to the following equations)

Since the curve is symmetry mirror to each other, the general equation for another curve could be easily obtained as:

$$x = e^t \cos t \quad (6)$$

$$y = -e^t \sin t \quad (7)$$

The differentials of two equations shown below:

From (4) and (5)

$$\frac{dy}{dx} = \frac{e^t \sin t + e^t \cos t}{e^t \cos t - e^t \sin t} \quad (8)$$

From (6) and (7)

$$\frac{dy}{dx} = \frac{-e^t \sin t - e^t \cos t}{e^t \cos t - e^t \sin t} \quad (9)$$

By the result above, it is easy to observe that the two curves will be remain perpendicular when the value of t in the general equation is same.

In our case, when these two polar equations have an intersection, the t values are same. Thus, the perpendicularity of general equation has been proved.

The differentials of two equations satisfied the condition of a pair of orthogonal trajectories, the gradients of every pair of intersecting curves are equal -1 . Thus, the curves will be remained as a set of orthogonal trajectories during the rotations respect to the common axis.

The advantages of using orthogonal trajectory is to stabilize the needle guide movement. When intersection remains as the small square shape due to the perpendicularity of two curves, the locations of those ball joints can be accurately determined.

2.1.3 Origin of Curve Developments

As we already introduced above, although the perpendicularity of two trajectory gives us considerable advantage. From the functional point of view, it is not completely necessary for the design of entire mechanism. To give origin of these curves discovery, other possible curves that may or may not fit into our application are discussed.

Starting from the simplest shape, putting linear grooves on the double disk, will not serve the function of restrain the ball joint. Essentially, as shown in the figure 5 (a), when the lines are generating from the origin, the rotation of disk will not move the position of intersection. When the lines are starting from other points on the disk, as shown figure 5 (b) and (c), bend at some point when it travels along the radius or combine with other curve shape. There might be a possibility for such combination to work out, however, the linear part will always cause the shape of intersection to change rapidly during the rotation of disk. A significant design issue can occurs when the linear edge reaches to be parallel with the edge on the other curve profile. Which causes the intersection wildly open and the ball joint will drop out upon this point. Thus, when designing this feature, linear shape less likely to be considered.

To study the curve design, a simple half circle curve was considered to understand the basic design limits (Shown in figure 5 (d). This shape will serve the purpose while the intersection travels on the middle part of curve. As the two curves are closing and the intersection reaching to the edge of each other, the two curves become tangential, which also forms the intersection widely open. Thus, while designing this feature, it was noted that the two curves shall never tangential to each other, and never even get close to tangential.

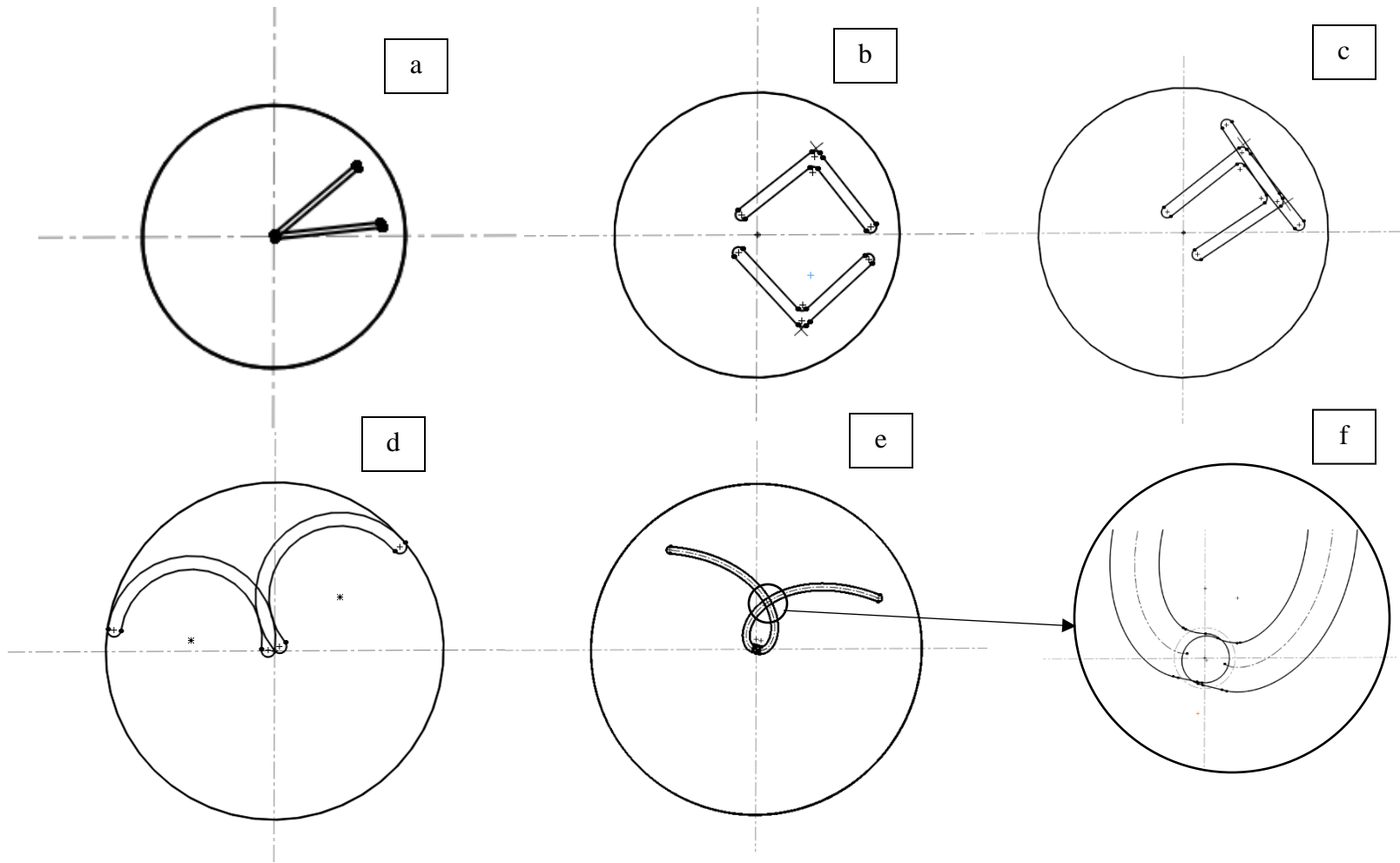


Figure 2-4 Illustration of few Design Discussion, (a) is linear shape (b) and (c) are linear shape with bending interruption, (d) is a half circle, (e) and (f) is for the center point discussion

With the consideration above, there are decent number of curves we could design to serve this function as long as the shape of intersection is carefully monitored. The angle between two curves upon the intersection does not have to equal to 90 degrees throughout the rotations. However, it needs to be controlled in a reasonable range close to 90 degrees. Considering the sliding of ball joints, it is hard to fix this angular range. Besides, such angular controls may also increase the complexity of control development.

For the curve profile that would fulfill such patterns, the curve turning angle must satisfy a pattern as follows: when the curve profile is close to the axis of disk, the angle of curve turning changes rapidly. Since it is close to the axis, maintaining the angle margins is difficult. When the curve profile is extending and close to the edge of disk, the angle of curve turning becomes slower. This feature is reasonable when it comes to maintain the perpendicularity between two curves, which is a feature of the function of:

$$R = e^t \quad (10)$$

(R here stands for the distance between axis and end point of curve for a particular value of t)

When t is smaller, R changes rapidly, and when t become a larger value, the R changes much slower.

Hence, when designing a new curve feature, the curve turning angle also needs to follow a similar principle. In our design, these two curves have been set up as theoretically perpendicular to each other. In which case, the ball joints forward and backward motion would experience similar amount of pushing forces and resistance. Hence, the motion of the ball joints would be smoother and control would also be simpler.

2.1.4 Issue with Center of Disks

As mentioned and shown in figure 2-4 (a), when using a center radiated linear shape to restrain the ball joint, the ball joint will not be able to leave the center point of the disk. For any curve profile including the one we selected, if the curve starts from the center of the disk, the ball joint will need an external support to leave the center point of the disk. As shown in the figure, when the ball joint moves to the center point of the groove, it will stop and stay. The grooves will lose their ability to control the ball joint because the center point of the disk is always an intersection. To help the ball joint leave the center point, an external spring structure can be added to push the ball joint out when the grooves start another rotation. However, to reduce the design complexity, the current design has disabled the pushing mechanism. The solution to control for the center point could be further established in future developments.

Finally, when it comes to the reason to design this polar coordinate system, it is essential to minimize the system volume and reduce the mechanism complexity. There are no extra components such as: robot arm, gearbox, or needle adaptation parts to add for this mechanism. Our design serves the current needle biopsy directly, the dimension of our mechanism is also close to the current manual template, which is already widely used in prostate biopsy. We believe all these advantages addressed will be favorable for potential users.

2.2 Design development

Prior to this article, our mechanism has been published as a concept idea and design mechanism development in both EMBC (Engineering in Medicine and Biology Society) [30]

In the EMBC [30], the abstract we published introduce the orthogonality of the two grooves and the principle of this mechanism. The design we developed for EMBC conference has been included in the APPENDIX A.

CHAPTER 3 CONTROL SYSTEM

3.1 Motion Control

For the motion control, we decided to use Galil motion controller, which is an industrial grade controller for advance motion control. The Galil motion controller DMC 4080 used for the system was chosen since it has four independent axis of motion control. The axis independent motion control from Galil is important for the system. For our application, the velocity profile for each motor is independent and complex. Each motor requires an independent motion control to deliver desired motion.

3.1.1 Decoupled simple motion control

Since the velocities of each motor are not uniform, it is easier to govern the motion using individual command. For two simple commands, each disk in one unit of double disks preforms symmetry motion with the other disk. First, let start with the pure rotation.

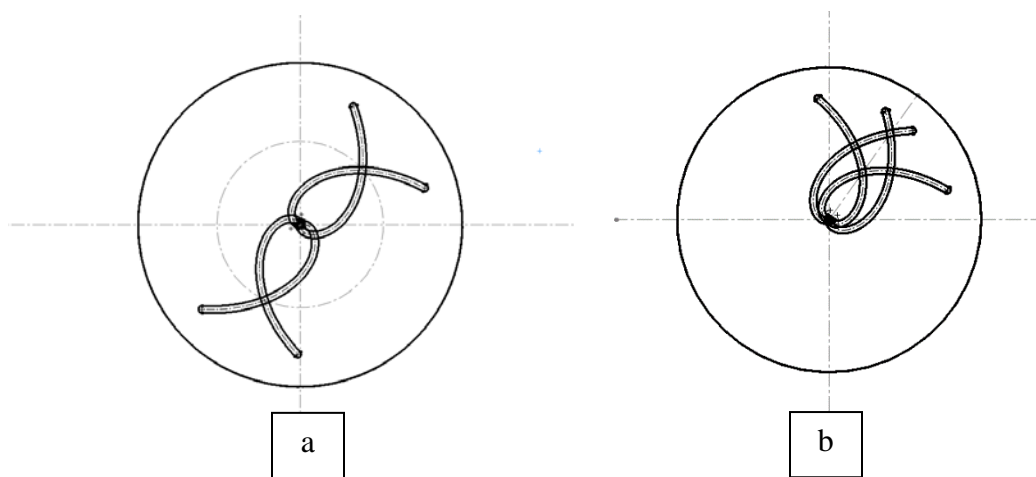


Figure 3-1 Two Simple Motion (a) Parallel Rotation, (b) Parallel Radius Motion

The pure rotation is to describe in one unit of double disk, the two disks are rotating in the same velocity and same direction. As shown in figure 6 (a), for this kind of motion, the intersection of the two groove is rotating in a constant radius respect to the center of disks. To conclude, the parallel rotation allows the intersection to travel through the entire radians for a known radius.

Another simple motion is the pure radius motion. As shown in figure 6 (b), in this case, for one unit of double disk, two disks in this unit are rotating in the same velocity but opposite direction. This kind of motion will make the intersection travel through the radius of the disk without changing the relative angular position. Hence, the parallel radius motion allows the intersection to change its rotation radius.

Under these two simple commands, the intersection of one unit of double disk can travel through the entire workspace on the 2-D plane. Thus, for those motion without requirement of continuous profile, the manipulation of simple command is sufficient for such cases. With two units of double disks, a 4-DOF decoupled motion control could be achieved by the combination of these two commands.

3.1.2 Continuous motion control

Considering continuous motion dynamic in our system, the motion profile for each motor is nonlinear. In order to drive the needle tip by a known uniform pattern, a complex and diverse motion profiles of the disks are needed. To observe the disks motion profile, we simulate the four disk motion scenarios by using SolidWorks motion study.

In the motion study, two units of double disk, two ball joints and a model of biopsy needle were used to determine the motion profile. The ball joint and grooves on the double disk are assembled by a path mate, in this path mate, the axis rotation of the ball joints is limited by 15-degree respect to the common disk axis.

The motion study has been illustrated below. First, the four disks have been adjusted to its homing position by using the homing mark show in the figure. Second, a path has been created on the target plane and defined as the needle tip path. A path mate is then created to connect the needle tip and this path on the target plane. Third, a path mate motor is defined to simulate the needle tip motions, by using the motion analysis of SolidWorks. After these features have been defined properly, the motion simulation was performed. The velocities of the four motors were also observed by using the motion analysis.

Once we obtain the angular velocity profile of the four disks from the motion study. We were able to calculate the motor velocity and position profiles by the integration of velocity and timing belt - pulley ratio. From this study, the disks' dynamics profile has been obtained (APPENDIX B).

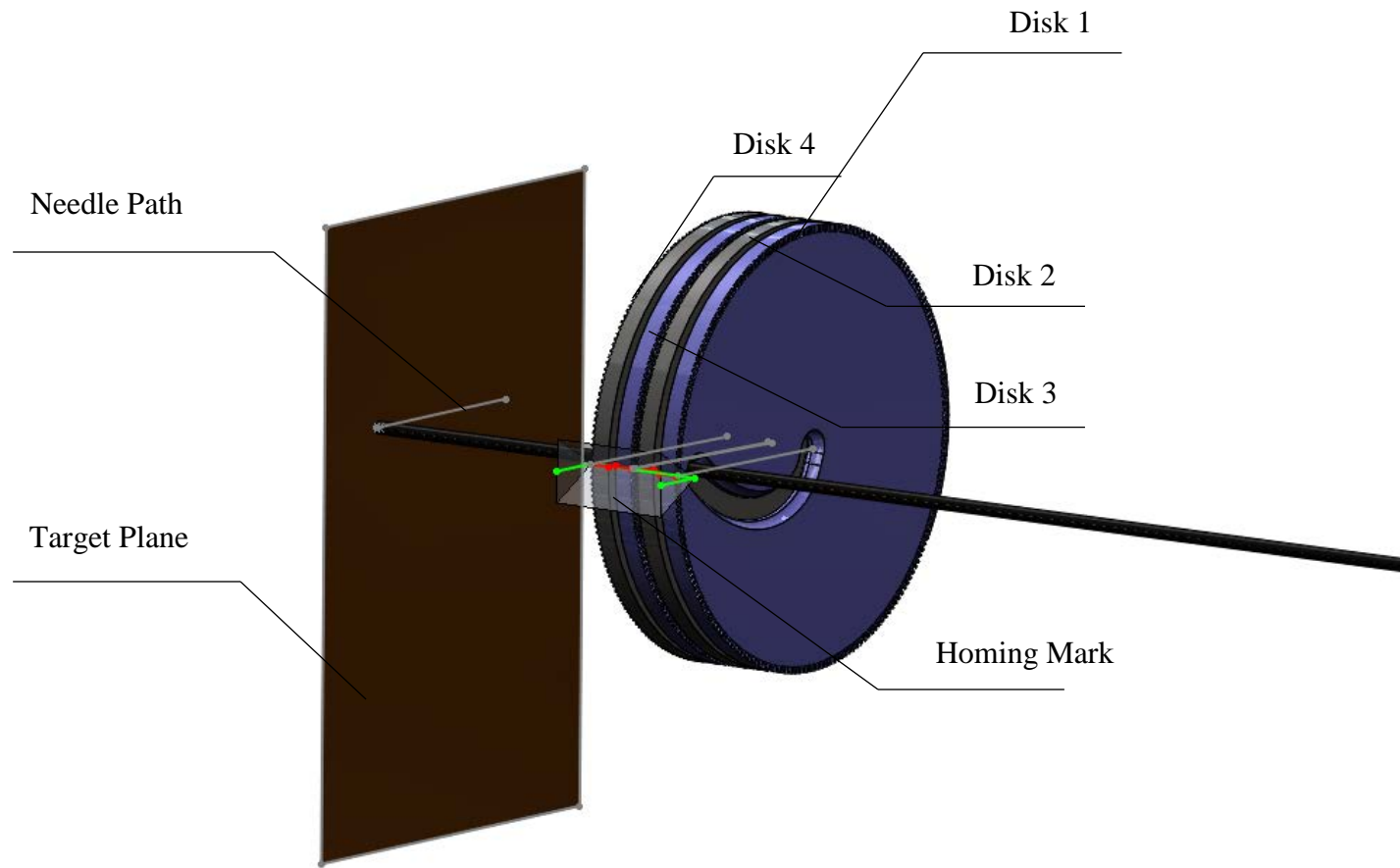


Figure 3-2 Configuration of Motion Study Setup

3.2 Homing Control

As shown in the SolidWorks motion study, prior to all the motion, four disks have to rotate to a known position. This position is critically important for the motion control since it is the reference for the disks' angular motion. In the motion study, the homing position is known by a homing mark. In real system, however, this homing position can be achieved by an optical sensing system (optical sensor and optical amplifier).

The optical sensor we used is able to emit a laser beam and also receive the reflection of that laser beam. Base on the strength of the reflection, the sensor is able to sense the position accordingly. In our system, the homing position will be marked by a high reflective color and the optical sensor will be installed to monitoring this color mark. In principle, once this high reflective color been delivered to the desire position, the optical sensor will feed a signal to the controller, the controller will set motors home position.

As showing in the figure 3-3, prior to the homing operation, the homing mark will be created on the timing belt for each of the belt and motor combinations. The optical sensor will also be installed to detect the reflection of the timing belt. During the homing control, the motors will be commanded to jog rotation to a distance of infinity, the velocity of the jog rotation will set to be less than 2 RPM for the disk. Once the homing mark has been detected by the optical sensor system, the optical sensor system will deliver a digital signal to the Galil controller. Once the Galil controller receives the signal, it will stop four motors immediately. The optical sensor we used for this application is Omron E32 series, with an amplifier Omron E3x series. Base on the manual, we designed the optical circuit, which is included in the APPENDIX C. The optical system we have can be taught to detect a particular reflection change. Those reflections below certain value will

be identified as low reflection. Otherwise, the reflection will be recognized as high reflection. In order to validate the controls, we used an oscilloscope to acquire the digital waveform from this optical sensing system. When lower reflection has been detected, the optical sensing system outputs a high signal. Once a higher reflection has been detected, the optical system delivers a low signal to the control output. The reading from the oscilloscope has been included in the APPENDIX C. This signal can be used to home the motors at desired position.

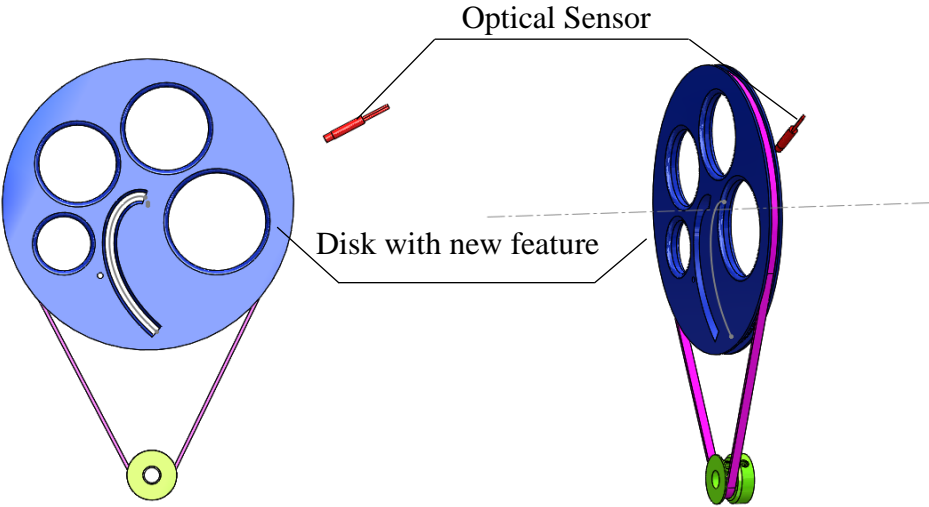


Figure 3-3 Homing System Setup

CHAPTER 4 DISCUSSION

In this these, a unique robotic mechanism for the MRI guided Intervention has been introduced. The target function of this mechanism is to guide a biopsy needle under MRI environment without any disruption in the current prostate biopsy clinical workflow under MRI imaging. Due to this requirement, the design feature focuses on designing a compact system that fits into the MRI bore and adapts to the current clinical setting. The compact feature of the system is critical due to the working conditions. The current MRI machines have limited bore dimensions. The typical dimension of the MRI bore is a diameter of 700 mm, with patient already fit inside. Consider such a limited space, the compact feature included in the design have significant advantages. The dimension of current design is also similar to the current TRUS biopsy manual template, which allows the MRI intervention to have required or greater accuracy and consistency from a robot guidance system. Considering the dynamics of the entire system, the intersections of each unit of double disk remain orthogonal regardless of the location of the intersection. This feature ensures the ball joints stability, also provides smooth planar movement. By the motion study, it was identified that needle could be continuously manipulated. In addition, after the needle being guided to the desire location, the non-back-drivability of the piezo motors will lock the position of needle. Thus, the clinician could hold this position while they need to perform other operations. This is also a favorable feature for the current clinician. While comparing with a fully automated needle manipulator, the system we proposed only assists clinicians. The final step, needle insertion is operated by qualified personnel. If any error occurs with the automatic robotic device, the clinician can terminate the operation. This approach has less safety concerns compared with the fully automated robots, since the human is in charge of the robotic operation. Overall, the system is able

to deliver position and angular guide to the MRI guided prostate intervention. The workspace of this device is sufficient for prostate needle insertion. By further development of the software, this intervention potentially can deliver needle guidance under real time MRI monitoring without interval.

On the other hand, the design of this concept has a few concerns. First, our system yet requires experiment to demonstrate and further prove its abilities. Further experiments are needed to verify the motion continuity, smoothness, and accuracy. Also, the MRI compatibility of entire system needs to be verified. Second, the velocity dynamics of the disks and motors will be another control challenge. The needle manipulation is critically relying on this complex velocity control. Besides, insuring the velocity patterns is also significant for the needle guide to move continuously and smoothly. For this concern, a Piezo LEGS motor, which can be operated under extremely low velocity, was selected since the entire system is supposed to run in a low speed. The higher accuracy of piezo motor should also reduce the difficulties of velocity control. From the SolidWorks motion study, it was confirmed that, while insuring continuous motion, the velocities of four disk could be adjusted to a relative uniform pattern. Hence, the velocity control for real time could be benefitted from this motion study.

The “center point” will raise another discussion for the system. During the development, the issue of the center point of the 4 disks has been removed from the robot workspace. However, the limitation does not necessarily limit the workspace of robot. As showing in the figure below, once a reasonable distance is provided between the robotic needle guide and the targeting prostate, the needle tip can still reach the common axis of the four disk which passes through the targeting area. The targeting area, which normally intersects with four disks’ common axis, does not need to be

excluded from the robot workspace. A rough estimation of the required distance mentioned above is greater than 60 mm[6] considering the needle can be only moved to a 15 degrees angle. It is also mentioned in previous publication that, the ball joint could be pushed out by a simple spring mechanism, which will increase the complexity of the disk components. This could be also considered as a solution for this concern.

CHAPTER 5 CONCLUSION

The concept and mechanism of the designed system is specifically aimed for satisfying the accuracy requirements in MRI guided needle placement. The MRI-guided targeted prostate biopsy has already been introduced in recent investigations and a number of biopsy needle guides have been introduced such as manual template, smart template and MrBot. The advantages of proposed MRI guided intervention are allowing the angular insertion and a compact size. The motor controls of proposed system require additional developments, and the dynamics of the disks in the design also needs to further research. The advantages of the purposed robotic intervention would allow the system to be integrated into existing clinical operation workflow without major changes. The MRI compatibility of the entire system could accelerate the adaptation of the MRI-guided targeted prostate biopsy, ultimately increasing prostate cancer detection rate in minimized time and cost.

APPENDIX A
PREVIOUS DESIGNED MECHANISM

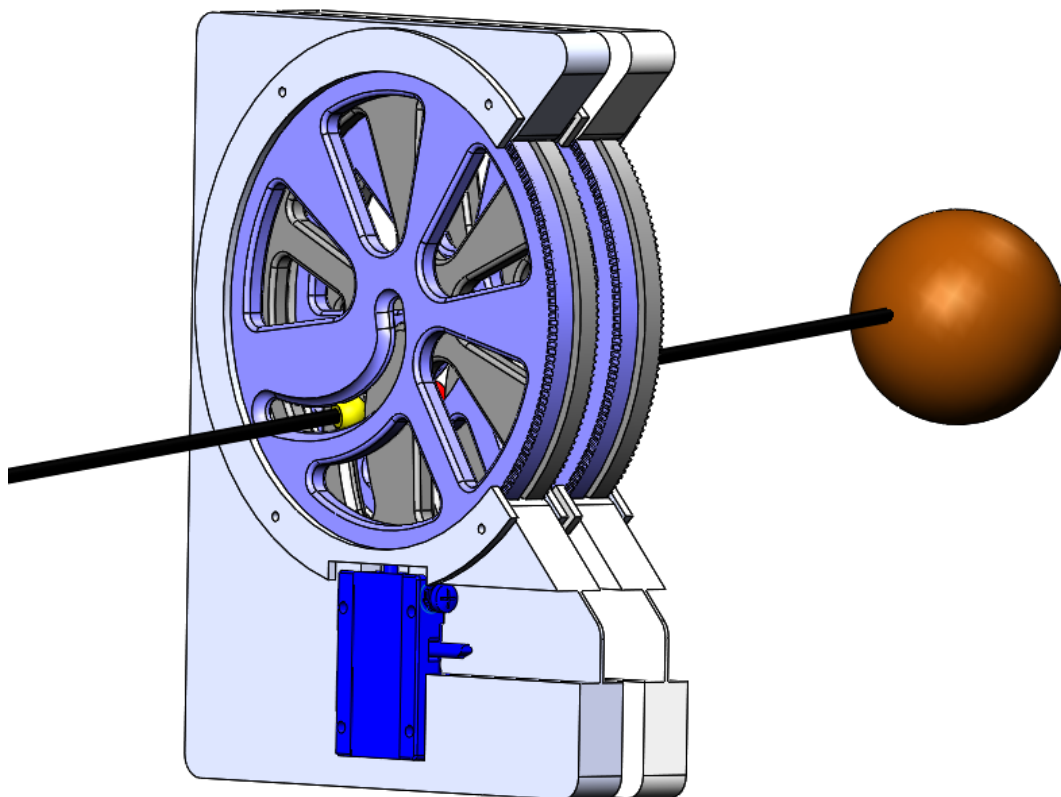


Figure 5-1 Previous Design Mechanism

A APPENDIX B
SOLID WORK MOTION STUDY

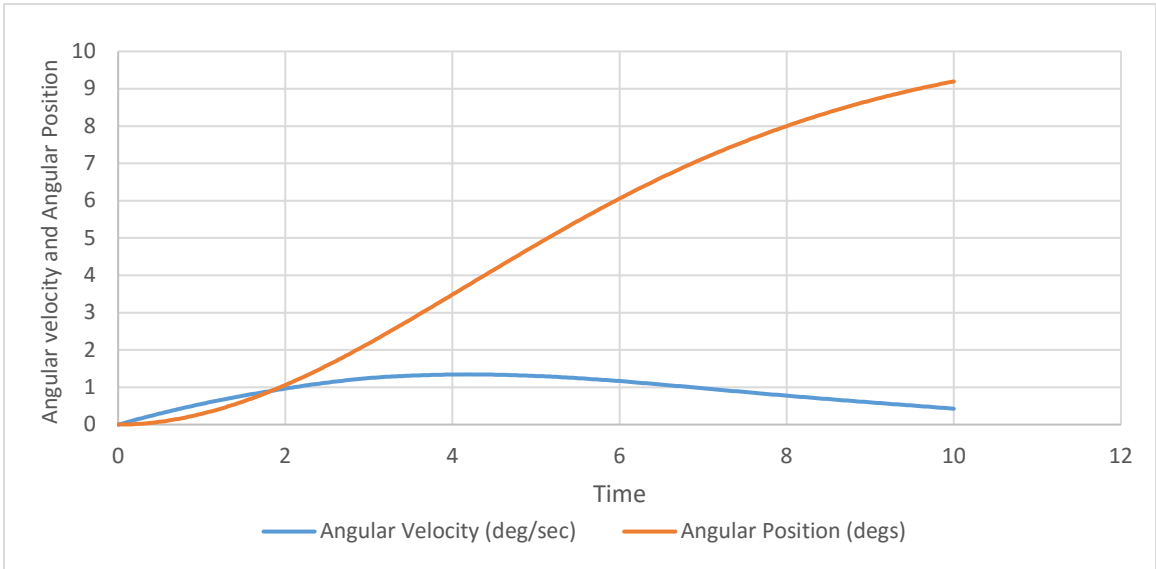


Figure 5-2 Disk 1 Dynamic for a Horizontal Linear Path

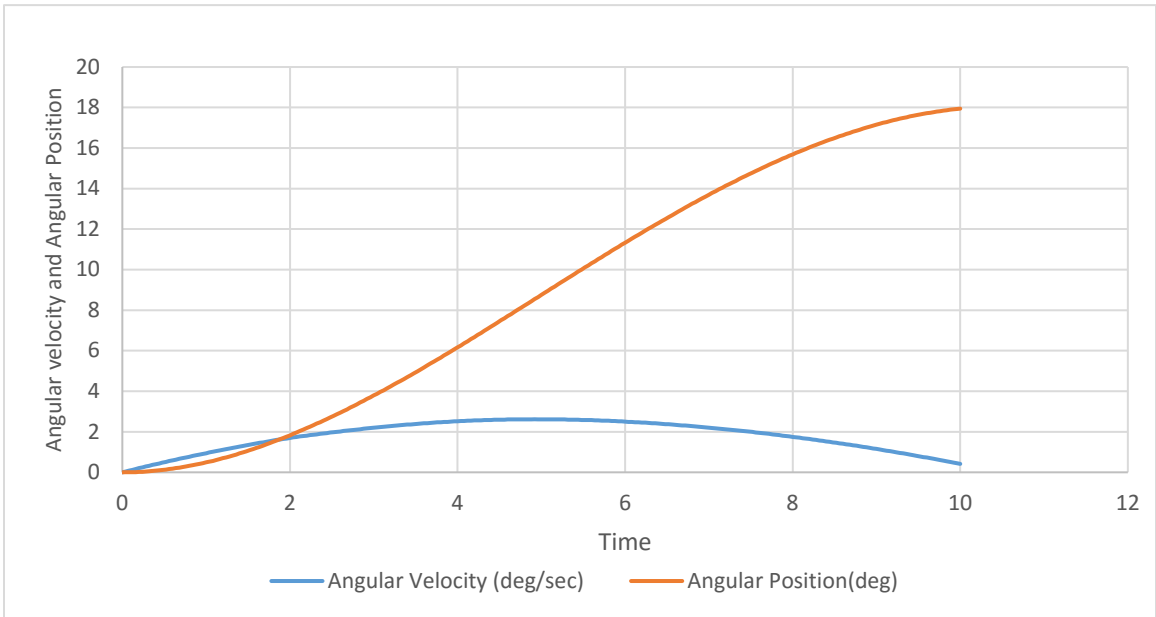


Figure 5-3 Disk 2 Dynamic for a Horizontal Linear Path

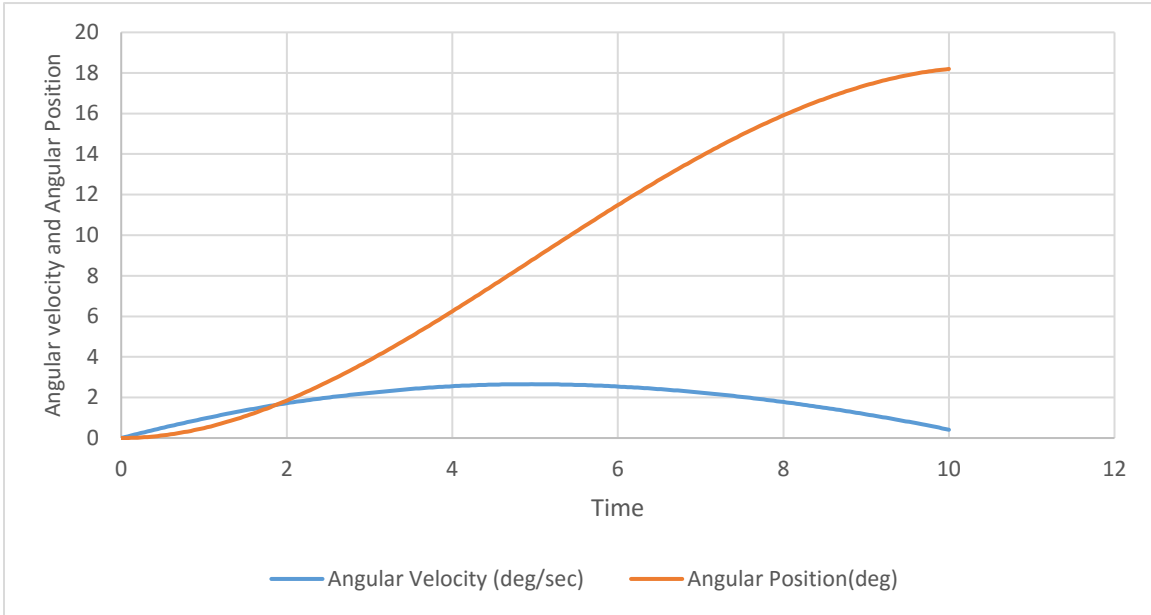


Figure 5-4 Disk 3 Dynamic for a Horizontal Linear Path

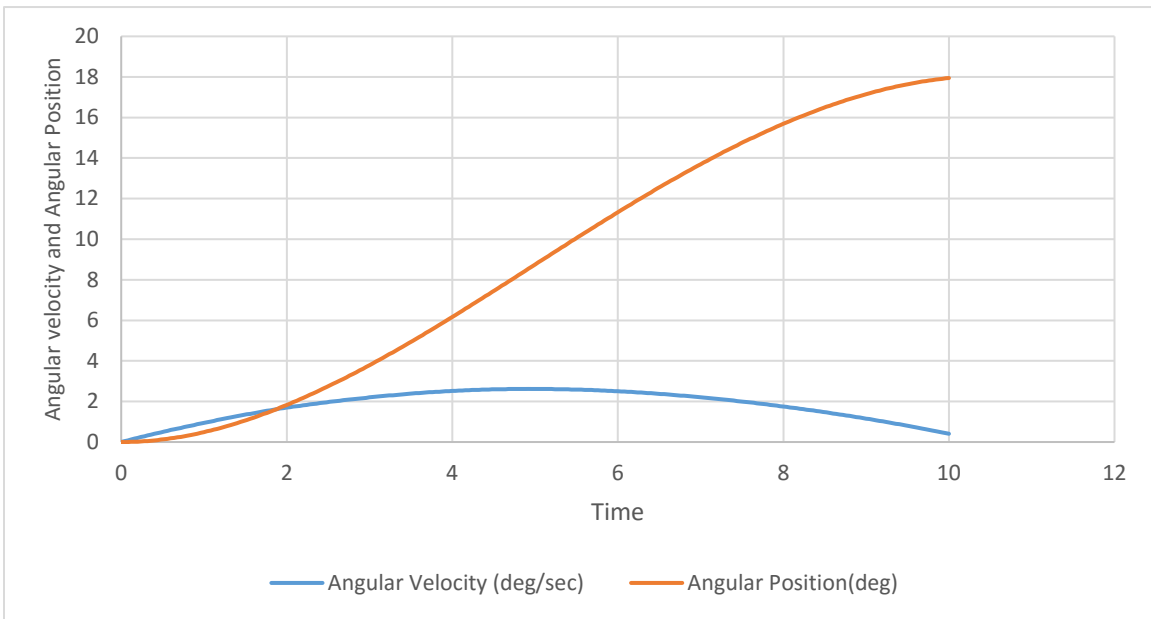


Figure 5-5 Disk 4 Dynamic for a Horizontal Linear Path

APPENDIX C
CIRCUIT AND OSCILLOSCOPE READING

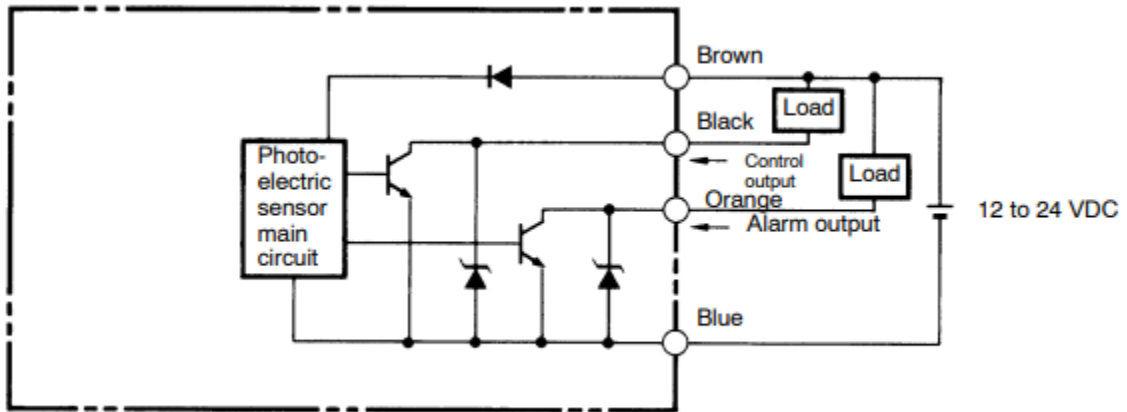
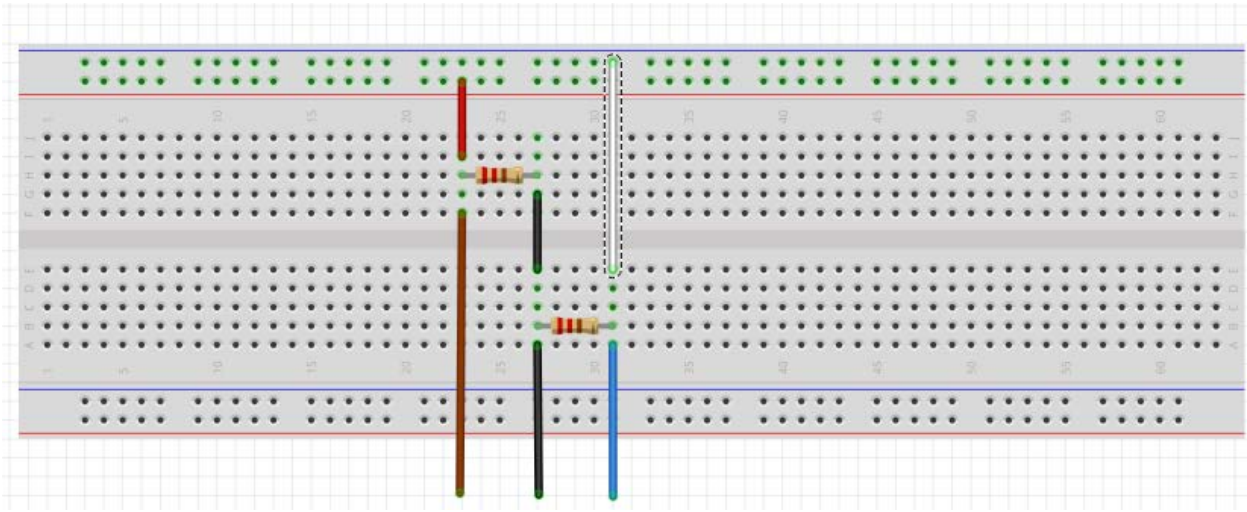


Figure 5-6 Circuit connection for E32 Optical Sensor

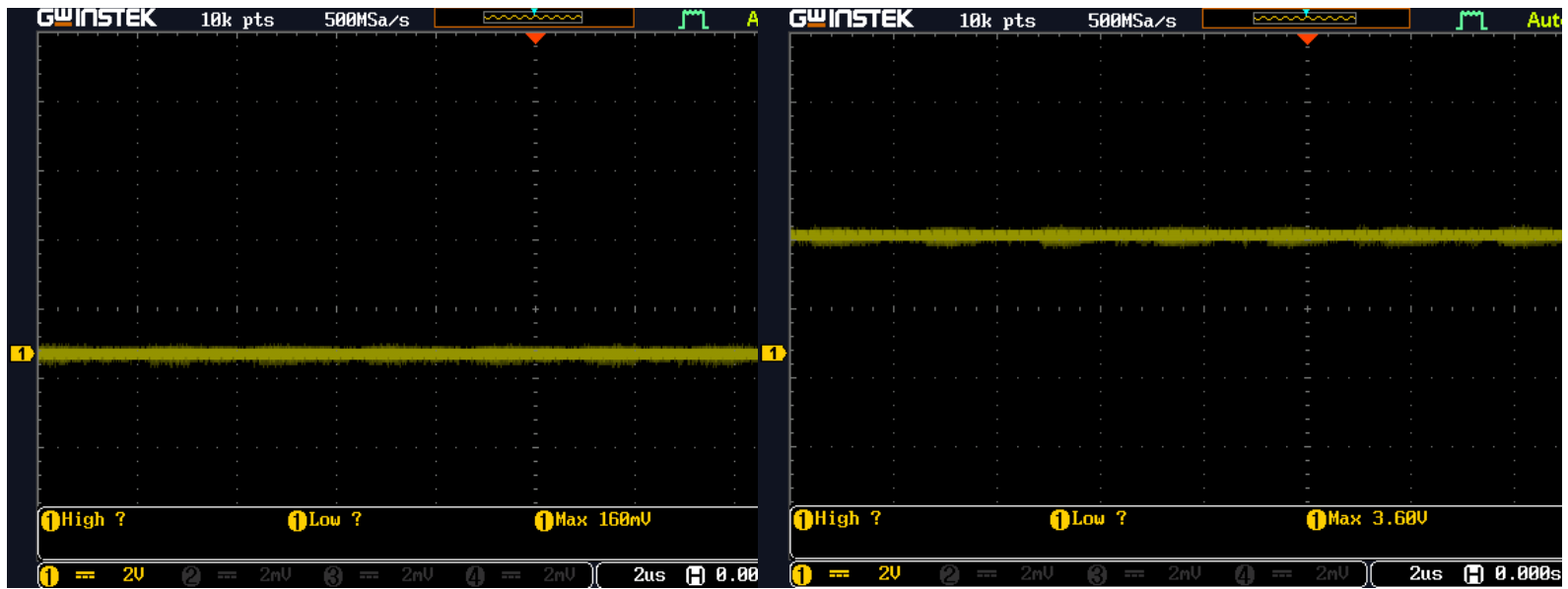


Figure 5-7 Oscilloscope Reading from the E-3-X Amplifier (a) Higher Reflection Detected, (b) Lower Reflection Detected

LIST OF REFERENCES

- [1] J. C. Miller and R. N. Uppot, "Multiparametric MR Imaging for Prostate Cancer," *Radiology Rounds*, vol. 8, p. 3, 2010.
- [2] G. Mohamed. Prostate Cancer. Available: <http://medicalechography.com/IMAGES/3KFneoprost.htm>
- [3] "Cancer Facts & Figures " American Cancer Society, 2018.
- [4] "Treating Prostate Cancer," American Cancer Society, 2018.
- [5] (2018). Prostate cancer prevention and early detection. Available: <https://www.seattlecca.org/diseases/prostate-cancer/early-detection-prevention>
- [6] N. Hata, I. Iordachita, A. Fedorov, J. Tokuda, K. Tuncali, S.-E. Song, et al., In-bore setup and software for 3T MRI-guided transperineal prostate biopsy.
- [7] E. C. Serefoglu, S. Altinova, N. S. Ugras, E. Akincioglu, E. Asil, and M. D. Balbay, "How reliable is 12-core prostate biopsy procedure in the detection of prostate cancer?," *Canadian Urological Association Journal*, vol. 7, pp. E293-E298, May-Jun 05/13 03/02/received 2013.
- [8] H. Wang, P. Nie, C. Dong, J. Li, Y. Huang, D. Hao, et al., "CT and MRI Findings of Soft Tissue Adult Fibrosarcoma in Extremities," *BioMed Research International*, pp. 1-7, 2018.
- [9] M. Roethke, A. G. Anastasiadis, M. Lichy, M. Werner, P. Wagner, S. Kruck, et al., "MRI-guided prostate biopsy detects clinically significant cancer: analysis of a cohort of 100 patients after previous negative TRUS biopsy," *World Journal of Urology*, vol. 30, pp. 213-218, 2012/04/01 2012.
- [10] S. S. Dianat, U. M. Hamper, K. J. Macura, H. B. Carter, E. M. Schaeffer, and J. I. Epstein, Association of quantitative magnetic resonance imaging parameters with histological findings from MRI/ultrasound fusion prostate biopsy.
- [11] C. M. A. Hoeks, J. O. Barentsz, T. Hambrock, D. Yakar, D. M. Somford, S. W. T. P. J. Heijmink, et al., "Prostate cancer: multiparametric MR imaging for detection, localization, and staging," *Radiology*, vol. 261, pp. 46-66, 2011.
- [12] "Development and Preliminary Evaluation of a Motorized Needle Guide Template for MRI-Guided Targeted Prostate Biopsy," *IEEE Transactions on Biomedical Engineering, Biomedical Engineering, IEEE Transactions on, IEEE Trans. Biomed. Eng.*, p. 3019, 2013.

- [13] N. Hata, I. Iordachita, A. Fedorov, J. Tokuda, K. Tuncali, S.-E. Song, et al., In-bore setup and software for 3T MRI-guided transperineal prostate biopsy, 2012.
- [14] D. Stoianovici, D. Song, D. Petrisor, D. Ursu, D. Mazilu, M. Mutener, et al., "'MRI Stealth" robot for prostate interventions," *Minimally Invasive Therapy & Allied Technologies*, vol. 16, pp. 241-248, 2007.
- [15] M. Schar and M. Schar, "MRI Stealth" robot for prostate interventions.
- [16] A. Krieger, S.-E. Song, N. B. Cho, I. Iordachita, P. Guion, G. Fichtinger, et al., "Development and Evaluation of an Actuated MRI-Compatible Robotic System for MRI-Guided Prostate Intervention," *IEEE/ASME Transactions On Mechatronics: A Joint Publication Of The IEEE Industrial Electronics Society And The ASME Dynamic Systems And Control Division*, vol. 18, pp. 273-284, 2012.
- [17] H. Dehghani, S. Zhang, P. Kulkarni, P. Biswas, L. Simms, and S.-E. Song, "Design and Simulation of Robotic Needle Guide for Transperineal Prostate Biopsy," *Proceedings of the 2018 Design of Medical Devices Conference*, 2018/04// 2018.
- [18] E. Bejer-Oleńska, M. Thoene, A. Włodarczyk, and J. Wojtkiewicz, "Application of MRI for the Diagnosis of Neoplasms," *BioMed Research International*, pp. 1-7, 2018.
- [19] J. Klostergaard, K. Parga, and R. G. Raptis, "Current and Future Applications of Magnetic Resonance Imaging (MRI) to Breast and Ovarian Cancer Patient Management," *Puerto Rico health sciences journal*, vol. 29, pp. 223-231, 2010.
- [20] S.-E. Song, J. Tokuda, K. Tuncali, C. Tempany, and N. Hata, "Development and preliminary evaluation of an ultrasonic motor actuated needle guide for 3T MRI-guided transperineal prostate interventions," *Proceedings of SPIE*, vol. 8316, p. 831614, 02/23/Number 1/February 2012 2012.
- [21] N. Hata, I. Iordachita, J. Tokuda, S.-E. Song, K. Tuncali, C. M. Tempany, et al., Preclinical evaluation of an MRI-compatible pneumatic robot for angulated needle placement in transperineal prostate interventions.
- [22] H. Su, W. Shang, G. Cole, G. Li, K. Harrington, A. Camilo, et al., "Piezoelectrically Actuated Robotic System for MRI-Guided Prostate Percutaneous Therapy," *IEEE/ASME Transactions on Mechatronics, Mechatronics, IEEE/ASME Transactions on, IEEE/ASME Trans. Mechatron.*, p. 1920, 2015.
- [23] Y. R. Guo and R. MacKinnon, "Structure-based membrane dome mechanism for Piezo mechanosensitivity," *eLife*, vol. 6, p. e33660, 12/12 11/17/received 12/11/accepted 2017.

- [24] PI Motion Positioning. Available: <https://www.physikinstrumente.com/en/technology/piezoelectric-drives/piezo-drive-technologies/>
- [25] S. Misra, T. Scheenen, H. Huisman, j. Futterer, D. G. H. Bosboom, J. Bomers, et al., Evaluation of a robotic technique for transrectal MRI-guided prostate biopsies.
- [26] PI-Medical Available: http://www.pi-medical.ws/products/piezo_actuators/product-overview.htm
- [27] (2010). The Mechanics of Medical Devices SHARE. Available: <https://www.medicaldevice-network.com/features/feature92861/>
- [28] PiezoMotor. Available: <https://www.piezomotor.com/>
- [29] S. D. Pathak, P. D. Grimm, V. Chalana, and Y. Kim, "Public arch detection in transrectal ultrasound guided prostate cancer therapy," IEEE Transactions on Medical Imaging, p. 762, 1998.
- [30] S. Zhang, E. S. Aldea, P. Biswas, L. Simms, S. Singh, M. Ortiz, et al., "Mechanism design of a compact 4-DOF robotic needle guide for MRI-guided prostate intervention," Engineering in Medicine and Biology Society, 2017.